coatings

MDPI

Article

Mathematical Modeling of Phase Separation and Branching Process of the Film Structure during Binary Thin Film Deposition

Gediminas Kairaitis [1], Matas Galdikas [1], Artūras Grigaliūnas [2] and Arvaidas Galdikas [1,2,*]

[1] Physics Department, Kaunas University of Technology, Studentu Str. 50, LT-51368 Kaunas, Lithuania; gediminas.kairaitis@ktu.lt (G.K.); matas.galdikas@ktu.lt (M.G.)
[2] Department of Physics, Mathematics and Biophysics, Lithuanian University of Health Sciences, Eivenių Str. 4, LT–50166 Kaunas, Lithuania; arturas.grigaliunas@lsmu.lt
* Correspondence: arvaidas.galdikas@ktu.lt

Abstract: In this study, we applied a mathematical model to explore the mechanism and factors leading to phase separation and the formation of branching structures with nanocolumns extending from larger clusters formed on the substrate of a grown film. The mathematical model simulated the growth of a thin film over time by using partial differential equations, including the processes of adsorption, phase separation, and diffusion due to the curvature of the thin film surface. The modeling results revealed the possible mechanism that could lead to the formation of the described branching structures. That mechanism can be divided into two main steps. The first step is the growth of a relatively large cluster (of a component that makes up the branching phase) on the substrate during the initial growth stages. The second step is the division process of that large cluster into smaller clusters in the later growth stages. The model parameters influencing the growth conditions that lead to the formation mechanism of the branching structures were determined, and their influences on the phase structure were analyzed.

Keywords: phase separation; kinetic modeling; thin films; surface roughness; compounds

Citation: Kairaitis, G.; Galdikas, M.; Grigaliūnas, A.; Galdikas, A. Mathematical Modeling of Phase Separation and Branching Process of the Film Structure During Binary Thin Film Deposition. *Coatings* **2022**, *12*, 610. https://doi.org/10.3390/coatings12050610

Academic Editor: Angela De Bonis

Received: 7 April 2022
Accepted: 28 April 2022
Published: 29 April 2022

1. Introduction

Nanocomposites, which are multiphase solid materials containing at least one phase with at least one dimension ranging from a few angstroms to a hundred nanometers, have attracted tremendous attention over the past few decades and have been recognized as one of the most promising materials systems for producing multifunctional properties [1,2]. A variety of nanocomposites containing or consisting of globular nanoparticles [3,4], nanocolumns [5,6], and layered structures [4,7] have already been fabricated and explored in many fields of application [2,5]. Chemico-physical properties of nanocomposites can be greatly influenced by nanoparticles size, shape, and mutual interactions [8], but the determination of two or more known substances and the preparation of nanostructures composed of those substances to optimally suit their applications, which usually encompasses the discovery of the optimal method and growth conditions, remain the challenging tasks. With the rapid development of nanoscience, encapsulation of nanoparticles has become an important issue. Encapsulation of nanoparticles in nanoshells or nanopores is expected to enable the physical isolation of nanoparticles, which could inhibit their migration and coalescence, making encapsulation a promising strategy to overcome various stability issues [9]. Various inorganic oxides, carbon, and organic cages can be used as encapsulating materials [9]. A better understanding of the mechanisms leading to the formation of a particular structure can help to obtain a better nanocomposite for a given application. A better understanding of nanocomposite growth mechanisms is usually

achieved through theoretical work dealing with the simulation of the growth of nanostructures.

There have been many recent works dedicated to the simulation of the growth of nanostructured thin films [10–21]. Much attention has recently been given to the nanostructures observed in Cu-Mo thin films [10,11,14,21], where approaches based on the phase field theory have been used to simulate the growth of thin films, with the modeling data mostly compared to the experimental data observed in Cu-Mo thin films. Determining the influence of deposition rate and substrate temperature on the phase structure in the Cu-Mo system [10,11] were the main objective in [10,11]. A morphology map as a function of deposition rate and mobility obtained from simulation data is provided by Ankit et al. in [11]. The influence of compositional variations within the vapor phase on the formation of hierarchical phase structures in co-deposited immiscible alloy thin films was investigated by Powers et al. in [14], where it was discovered that certain vapor phase compositions promote the development of hierarchical structures during co-deposition of the alloy thin film. The effects of temperature-dependent surface and bulk diffusivities, temperature-dependent thermodynamic driving force for phase separation, and composition-dependent interfacial and surface energies on the phase structure of immiscible alloy thin films were investigated in [21]. A phase structure containing V-shaped nanocolumns elongated in the growth direction was reproduced with the simulations use of a kinetic Monte Carlo approach by Perzynski in [12], where it was determined that the kinetic Monte Carlo method can provide a good representation of structures formed in TiN thin film grown by the pulsed laser deposition method. Kinetic Monte Carlo approaches were also used to investigate the influence of substrate tilt angle [15], substrate temperature [16], deposition rate [12], and composition ratios [17] on the phase structure of nanocomposites. The influence of substrate tilt angle on the surface roughness and the tilt angle of TiN columns was analyzed by Bouaouina et al. in [15]. A molecular dynamics approach [18] proposed by Zhou et al. was employed to investigate the factors influencing stress generation in body-centered cubic metal thin films. Stewart and Dingreville [19] analyzed the influences of deposition rate, dissimilar bulk and surface kinetics, phase fraction, and dissimilar elastic response on thin film microstructure during simulated physical vapor deposition. The influences of substrate temperature, incoming ion fluxes, and growth rate on phase structure and surface roughness of grown films were examined in our previous works [13,20]. By using models based on phase field theory, both works revealed the relationships between substrate temperature and average lateral dimensions of nanoparticles formed during film growth. The relationships between average lateral dimensions of nanoparticles and surface roughness were also reported in our previous works; both surface rougnesses of grown films and average lateral nanoparticle size tended to increase as the substrate temperature rose.

The purpose of this work was to reveal and explain the mechanism leading to the formation of branching morphologies, which have been observed in yttrium-stabilized zirconia thin films (see Figure 11 in [22] or Figure 1b in [23], where the branching structures with nanocolumns extending from larger clusters formed on the substrate to the surfaces of the grown film were observed). A modification of the previously used mathematical models [13,20] was used to simulate the growth processes in three spatial dimensions and time. The model includes the processes of phase separation, adsorption, and diffusion due to surface curvature (of a growing film). A possible mechanism of the formation of branching structures reported in [22,23] was revealed by our modeling results. The physical processes that promote that mechanism were distinguished, and their influences on the formation of such branching structures were revealed by the modeling results.

2. Materials and Methods

We employed a three-dimensional grid to simulate the growth processes of a thin film in three spatial dimensions and time. The composition of a growing thin film in a modeling domain is described by using the relative concentrations of thin film components. Three local relative concentrations $c_A^{i,j,k}$, $c_B^{i,j,k}$, $c_S^{i,j,k}$, i = 1,..., I, j = 1,..., J, k = 1,..., K, were associated with each grid point, and they represented the concentrations of components A, B, and substrate material, respectively, at grid point i, j, k. The indices i, j specified the positions of a respective grid cell in the horizontal directions, k indicating the position in the vertical direction that was the film growth direction. The condition $c_A^{i,j,k}+c_B^{i,j,k}+c_S^{i,j,k} \leq 1$ was always met in any grid cell. A modification of previously published models [20] was employed in this work to simulate the growth processes of thin films. The modified model still includes the processes of phase separation, diffusion of both thin components due to surface curvature, and adsorption. The mathematical description of the phase separation of both components occurring through the surface diffusion was based on the Cahn–Hilliard equation [24] and on the idea presented in our previous work [20]. The present model uses the same equation and variables as those used in [20] to obtain a mathematical description for the phase separation; however, the present model is constructed slightly differently. Changes in the concentrations of component A due to phase separation in the surface layer of a growing film were described by the following equation [20]:

$$\frac{\partial c_{AS}}{\partial t} = \nabla D_A \nabla \left(\frac{df(c_{AS})}{dc_{AS}} - \gamma \nabla^2 c_{AS} \right) \quad (1)$$

where c_{AS} ($c_{AS}^{i,j}, i = 1,\ldots,I, j = 1,\ldots,J$) denotes the concentrations of component A in the film surface cells, D_A is the diffusion coefficient, $f(\varphi) = 2(2\varphi^{10} - \varphi^8 - \varphi^6 - \varphi^4 - \varphi^2 + 2)$ is the function of the free-energy density of a homogenous system (the even function $f(\varphi)$ used in this work is same as that used in [25], which is related to the solubilities of components in a binary system), and γ is the power coefficient of the phase gradient. The concentrations of component A in the surface layer, $c_{AS}^{i,j}$ (this is the concentration variable used in Equation (1)), is defined through by following relation [13,20]:

$$c_{AS}^{i,j} = c_A^{i,j,k^*} \quad (2)$$

where k^* is the highest position (in the growth direction) at which $c_A^{i,j,k}+c_B^{i,j,k}+c_S^{i,j,k} > 0$ is satisfied.

The diffusion coefficient of component A denoted by D_A (for each surface cell of a film, $D_A = D_A^{i,j}, i = 1,\ldots,I, j = 1,\ldots,J$) is defined as a weighted average by the following equation:

$$D_A = D_{AA}c_{AF} + D_{AB}c_{BF} + D_{AS}c_{SF} \quad (3)$$

where D_{AA}, D_{AB}, and D_{AS} are the diffusion coefficients of component A on pure phase A, phase B, and substrate material, respectively. The weights c_{AF}, c_{BF}, c_{SF} are the surface relative concentrations (they are assessed considering the one full surface layer) of component A, component B, and substrate material, respectively, and they are defined for each grid surface cell separately by the following relationships [20]:

$$\begin{aligned} c_{AF}^{i,j} &= c_A^{i,j,k^*} + c_A^{i,j,k^*-1}(1 - c_A^{i,j,k^*} - c_B^{i,j,k^*} - c_S^{i,j,k^*}), \\ c_{BF}^{i,j} &= c_B^{i,j,k^*} + c_B^{i,j,k^*-1}(1 - c_A^{i,j,k^*} - c_B^{i,j,k^*} - c_S^{i,j,k^*}), \\ c_{SF}^{i,j} &= c_S^{i,j,k^*} + c_S^{i,j,k^*-1}(1 - c_A^{i,j,k^*} - c_B^{i,j,k^*} - c_S^{i,j,k^*}). \end{aligned} \quad (4)$$

From the relationships given in Equation (4) the relative concentration of component A (considering the one full surface layer) is $c_{AF}^{i,j} = c_A^{i,j,k^*}$ if the surface site, i,j, is full ($c_A^{i,j,k^*} + c_B^{i,j,k^*} + c_S^{i,j,k^*} = 1$); if that site is not full ($c_A^{i,j,k^*} + c_B^{i,j,k^*} + c_S^{i,j,k^*} < 1$), the concentration, $c_{AF}^{i,j}$, is defined as the sum of the concentrations of component A from the respective

highest occupied grid cell denoted by i, j, k^* and the one grid cell below it indicated by $i, j, k^* - 1$. The process of phase separation described by Equation (1) ensures that atoms of type A adsorbed and migrating on any nanoisland (made either of component A or B) or on substrate material gather together and can form fully filled grid cells made of component A. This process can occur on a substrate material, on nanoislands made of component A, on nanoislands made of component B, or on any surface made of their mix, so the diffusion coefficient, D_A, is expressed as a weighted average of D_{AA}, D_{AB}, and D_{AS} (the diffusion coefficients of component A on pure phase A, phase B, and substrate material, respectively). To define the process of phase separation for component B, we also employ Equation (1), but we use the concentration variable, c_{BS} (denotes concentrations of component B in the film surface cells), and the diffusion coefficient, D_B, instead of c_{AS} and D_A, respectively. The variables c_{BS} and D_B can also be defined from Equations (2) and (3) by adjusting them to be suitable for component B:

$$\begin{gathered} c_{BS}^{i,j} = c_B^{i,j,k^*}, \\ D_B = D_{BA}c_{AF} + D_{BB}c_{BF} + D_{BS}c_{SF}, \end{gathered} \tag{5}$$

where k^* is the highest position (in the growth direction) at which $c_A^{i,j,k} + c_B^{i,j,k} + c_S^{i,j,k} > 0$ is satisfied. D_{BA}, D_{BB}, and D_{BS} are the diffusion coefficients of component B on pure phase A, phase B, and substrate material, respectively. The concentrations c_{AF}, c_{BF}, c_{SF} are defined by Equation (4).

The diffusion of atoms on nanoislands due to their surface curvature is another process included in the model [26]. Changes in the concentrations of component A due to the surface curvature of a growing film were defined by using the following equation [20] (the mathematical description of this process is the same as that in [20]):

$$\frac{\partial c_{AS}}{\partial t} = \nabla D_A \nabla(-p_A c_{AS} \nabla^2 h) \tag{6}$$

The term $\nabla^2 h$ denotes that the surface curvature, h, was the position of the thin film surface, and p_A was the proportionality coefficient. Equation (6) ensures that atoms of respective type diffuse from crests to valleys of nanoislands due to the surface curvature. Equation (6) also defines changes in the concentrations of component B due to the surface curvature, but c_{BS}, p_B, and D_B have to be used instead of c_{AS}, p_A, and D_A, respectively, in Equation (6).

Changes in the concentrations of both depositing species (at the highest occupied surface cells c_A^{i,j,k^*}, c_B^{i,j,k^*}) caused by the adsorption process were described by using the following equations [20] (the mathematical description of this process is same as in [20]):

$$\begin{gathered} \frac{\partial c_A^{i,j,k^*}}{\partial t} = k_{AA} i_A c_{AF}^{i,j} + k_{AB} i_A c_{BF}^{i,j} + k_{AS} i_A c_{SF}^{i,j}, \\ \frac{\partial c_B^{i,j,k^*}}{\partial t} = k_{BA} i_B c_{AF}^{i,j} + k_{BB} i_B c_{BF}^{i,j} + k_{BS} i_B c_{SF}^{i,j}, \end{gathered} \tag{7}$$

where i = 1,..., I, j = 1,..., J, k_{AA}, k_{AB}, and k_{AS} are the sticking coefficients (k_{AB} denotes the sticking coefficient of A-type atoms to the surface made of component B); and i_A and i_B are the relative fluxes of both film components; $c_{AF}^{i,j}$, $c_{BF}^{i,j}$, and $c_{SF}^{i,j}$ are the surface concentrations of components A, B, and substrate material, respectively. The sum, $\partial c_A^{i,j,k^*}/\partial t + \partial c_B^{i,j,k^*}/\partial t$, amounted to the total growth rate of the thin film.

All the three equations describing the three different processes with respect to the film component were added together to obtain the final model for that component. Because we investigated two growing phases, the two separate models dealing with each growing phase and consisting of Equations (1), (6) and (7) were employed. Our previous model [20] used the two Cahn–Hilliard equations for each component, so it consisted of the four summands.

3. Results and Discussion

To investigate and determine factors resulting in the growth of branching structures, a series numerical experiments was performed. The lateral dimensions of the simulation domain were 36 nm × 36 nm, and the spacing of the computational grid was 1 nm. The boundaries of the simulation domain parallel to the growth direction were used as the periodic boundary conditions. In the simulation domain, the substrate was represented as five perfectly flat layers occupying those layers counting from the bottom of the simulation domain. The basic values of the parameters used in calculations are given in Table 1.

Table 1. Values of model parameters used in calculations.

Model Parameter	Value	Unit
D_{AA}, D_{BB}	2.2×10^{-19}	m^2/s
D_{AB}, D_{BA}	8.8×10^{-19}	m^2/s
D_{AS}	8.8×10^{-17}	m^2/s
D_{BS}	2.2×10^{-18}	m^2/s
k_{AA}, k_{AB}, k_{BA}, k_{BB}	0.5	r.u.
k_{AS}	0.75	r.u.
k_{BS}	0.15	r.u.
i_A	0.2666	s^{-1}
i_B	0.5333	s^{-1}
p_A, p_B	2.4×10^{-14}	J/m
γ	4.8×10^{-13}	J/m

The parameters D_{AA}, D_{BB}, D_{AB}, D_{BA}, k_{BA}, k_{BB}, i_A, i_B, p_A, p_B, and γ were kept constant in all calculations. Some of those parameter values are consistent with those used in our previous works [13,20,27]. As shown by [27], the diffusion values similar to those of D_{AB} and D_{BA} given in Table 1 resulted in the formation of columnar structures throughout the whole film thickness (diffusion coefficients D_{AB} and D_{BA} determine the phase separation rate in the later growth stages when the substrate is covered with depositing species). The presence of nanocolumns was also observed in the branching structures being considered. The diffusion coefficients D_{AA} and D_{BB} were chosen of the same order as D_{AB}, D_{BA}. The values of p_A and p_B used in this work were lower than those used in our previous works [13,20]. Those parameters determine the diffusion on nanoislands due to their surface curvature. The influence of that effect was not investigated in this work, so the relatively smaller values of p_A and p_B were used. The parameters D_{AS}, D_{BS}, k_{AA}, k_{AB}, k_{AS}, and k_{BS} were varied in respective numerical experiments. Any changes in their values will be specified.

Figure 1 shows horizontal (Figure 1a–c,e–k) and vertical (Figure 1d,h,l) cross sections through multiple planes obtained by using different diffusion coefficients of component A on the substrate material. The values of the diffusion coefficient were as follows: D_{AS} = 8.8×10^{-17} m^2/s (Figure1a–d), D_{AS} = 2.2×10^{-17} m^2/s (Figure 1e–h), and D_{AS} = 8.8×10^{-19} m^2/s (Figure1i–l). In horizontal cross sections, red–brown color marks regions made of pure component A, and blue color represents regions made of pure component B. The horizontal cross sections are given through the planes z = 6 (Figure 1a,e,i), z = 12 (Figure1b,f,j), and z = 18 (Figure 1c,g,k). The horizontal cross sections through the plane z = 6 reflect the distributions of both thin film components on the layer situated on top of the substrate (the first five layers counting from z = 1 are the substrate material). The horizontal cross sections through the plane z = 18 represent the distributions of both thin film components on the layer near the surface of the film grown, and the cross sections through the plane z = 12 show the distribution of both component in the layer that can be considered to be situated in a mid-depth of the films grown. In the vertical cross sections, red–brown color marks the substrate material, orange color represents regions made of pure component A, and light green color indicates regions made of pure component B. All the vertical cross

sections are shown through the same plane, x = 15. According to comparisons of the images in Figure 1a,c,i, the largest clusters (with respect to their lateral dimensions near the substrate) of component A are observed at the highest value of the diffusion coefficient, D_{AS}. It should be noted that the periodic boundary conditions are used at the boundaries x = 1, x = 16, y = 1, and y = 36, so in Figure 1a, those boundaries only visually divide all the clusters formed on the substrate. The relationship between lateral dimensions of nanoparticles made of some component and diffusion coefficient of that component was also observed in other works [13,20,28,29]. From the images in Figure 1a–d it can be seen that the relatively large nanoclusters made of component A (with respect to the lateral dimensions) formed during the initial stages of the growth do not keep their lateral sizes throughout the whole film thickness, and the large clusters of component A formed on the substrate material start to branch into smaller ones. In the vertical cross section in Figure 1d, we observe relatively narrow elongated (in the growth direction) nanoparticles made of component A grown from a basic relatively large nanocluster formed in the initial stages of film growth. As can be seen from Figure 1d, the smaller nanoparticles of pure phase A remained connected to the large cluster made of phase A. As the image in Figure 1d suggests, such a branching process started to occur right after the majority part of the substrate had been covered with either phase A or B, so this branching process must be related to some different growth mechanisms resulting in the growth of different structures in the early and later growth stages. Judging from the values of the parameters used in the calculations presented in Figure 1, besides the relatively high value of D_{AS} (the diffusion coefficient of component A on the substrate material is two orders of magnitude higher than the diffusion coefficients of component A on pure phases of A and B) used to generate the images in Figure 1a–d, the sticking coefficient of component A to the substrate material was set to 0.75, whereas the sticking coefficient of component B to the substrate material was 0.15. Those values of the sticking coefficients were kept as constants for all calculations in Figure 1. Therefore, the formation of relatively wide clusters of component A on the substrate in the early growth stages is influenced by two factors. The first is the relatively high diffusion coefficient of component A on the substrate material. The second factor is the higher value of the sticking coefficient of component A to the substrate material than the sticking coefficient of component B to the substrate material. The influence of the value of the diffusion coefficient of component A on the substrate material is further shown in Figure 1e–l, where the structures obtained with $D_{AS} = 2.2 \times 10^{-17}$ m²/s (four times lower than the initial value, 8.8×10^{-17} m²/s) and $D_{AS} = 8.8 \times 10^{-19}$ m²/s (100 times lower than the initial value) are presented. According to Figure 1e–h, the four-times lower diffusion coefficient, D_{AS}, reduces the dimensions of nanoparticles of component A formed on the substrate material by two to three times. However, as can be seen from the images in Figure 1g,h, the branching process still occurred. Figure 1h suggests that smaller lateral dimensions of initial clusters of component A formed on the substrate result in a smaller number of elongated nanoparticles of component A extending from those initial clusters to the surface of the grown film. Figure 1i shows that the further decrease in the diffusion coefficient, D_{AS}, to 8.8×10^{-19} m²/s changed the structure formed on the substrate very significantly. As can be seen in Figure 1i, there are no encapsulated nanoparticles of component A in the given horizontal cross section through the plane z = 6 (with respect to the horizontal directions); the clusters made of component A are connected to one another. This behavior is caused by a relatively high concentration of phase A grown on the substrate material and by a relatively low value of the diffusion coefficient of component A on the substrate material, D_{AS} ($D_{AS} = 8.8 \times 10^{-19}$ m²/s used to calculate Figure 1i–l was lower than the value of D_{BS}, which was kept constant in the presented calculations). As shown by the images in Figure 1j,k, although the composition of the thin film obtained with the lowest diffusion coefficient D_{AS} in the mid-depth and surface layers remain similar to the cases obtained by using the higher diffusion coefficient D_{AS}, the phase structures of layers grown on the substrate are quite different. As shown by the vertical cross section

given in Figure 1l, no distinguishable branching structures can be observed at the relatively low value of D_{AS}.

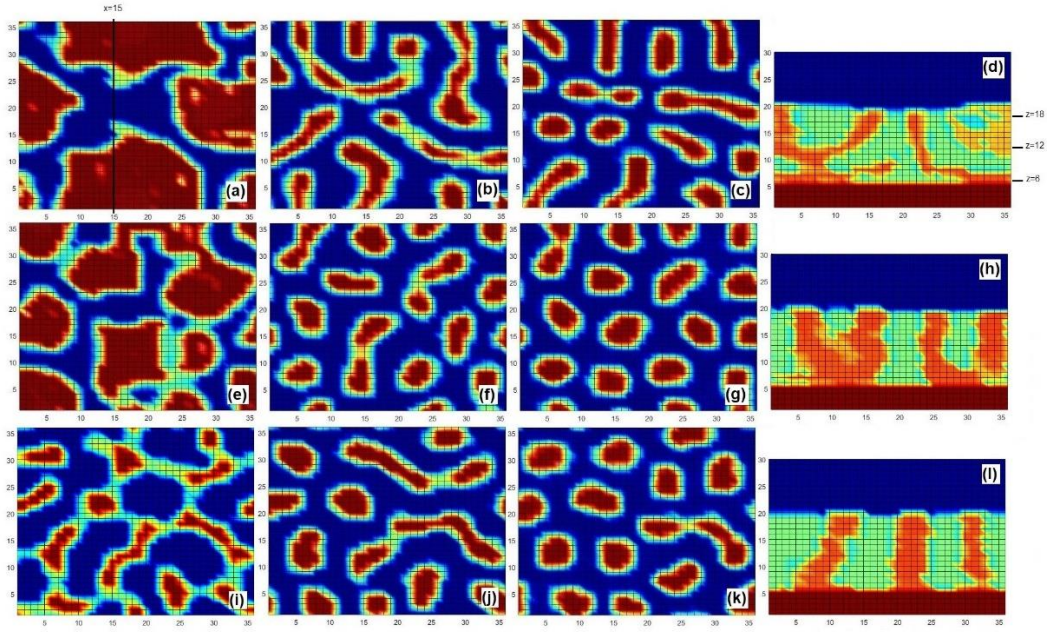

Figure 1. Horizontal cross sections through the planes z = 6 (**a**,**e**,**i**), z = 12 (**b**,**f**,**j**), and z = 18 (**c**,**g**,**k**) and vertical cross sections through the plane x = 15 (**d**,**h**,**l**) obtained with the following diffusion coefficient values of component A on substrate material: $D_{AS} = 8.8 \times 10^{-17}$ m^2/s (**a**–**d**), $D_{AS} = 2.2 \times 10^{-17}$ m^2/s (**e**–**h**), and $D_{AS} = 8.8 \times 10^{-19}$ m^2/s (**i**–**l**).

As previously mentioned, the formation of the branching structures observed in Figure 1a–h was not only influenced by the diffusivities of deposited components on the substrate material but also by the values of the sticking coefficients. Figure 2 shows horizontal and vertical cross sections obtained by using different sticking coefficients of components A and B to the substrate material. All the other model parameters were the same as those used to calculate the structure in Figure 1a–d, so those images are comparable to the respective images in Figure 2. The values of the sticking coefficients were as follows: k_{AS} = 0.75, k_{AB} = 0.15 (Figure 1a–d), k_{AS} = 0.6, k_{AB} = 0.3 (Figure 2a–d), k_{AS} = 0.45, and k_{AB} = 0.45 (Figure 2e–h). The sum of sticking coefficients k_{AS} and k_{AB} was kept constant in the given series of the calculations, but the differences between those coefficients were varied. The horizontal cross sections of Figure 2 are given through the same planes z = 6 (Figure 2a,e), z =12 (Figure 2b,f), and z = 18 (Figure 2c,g) as in Figure 1. The vertical cross sections of Figure 2 are given through the planes x = 27 (d) and x =15 (h), which ensured a good representation of the structures formed.

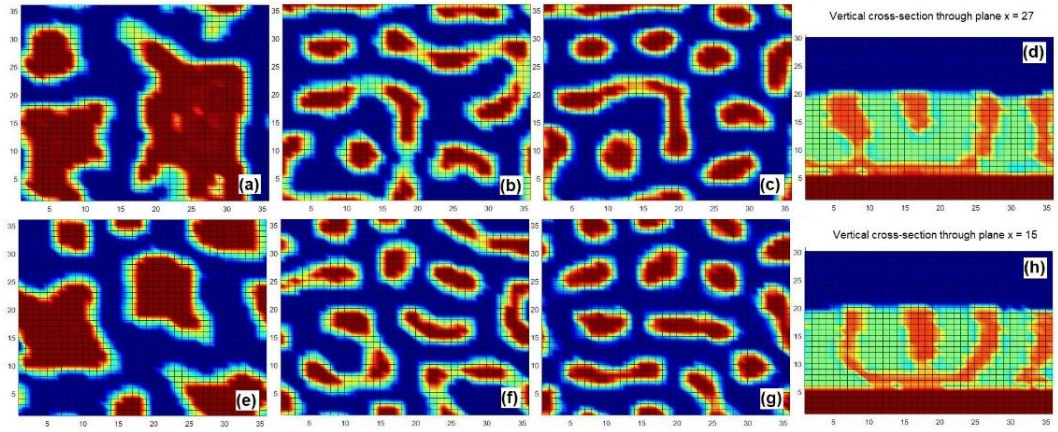

Figure 2. Horizontal cross sections through the planes z = 6 (**a**,**e**), z =12 (**b**,**f**), and z = 18 (**c**,**g**) and vertical cross sections through the planes x = 27 (**d**) and x = 15 (**h**) obtained with the following sticking coefficients: k_{AS} = 0.6, k_{AB} = 0.3 (**a**–**d**), k_{AS} = 0.45, and k_{AB} = 0.45 (**e**–**h**).

Comparing the images in Figures 1a and 2a,e, we notice that such a change in the value of the sticking coefficient of component, A, to the substrate , k_{AS} (keeping the sum $k_{AS} + k_{BS}$ constant), clearly has an influence on the phase structures formed on the substrate. In all the three cases shown in Figures 1a and 2a,e, we observe groups of clusters of component A formed on the substrate. The average lateral sizes of clusters of component A (calculating their sizes in the plane z = 6) are as follows: 17.8 nm (in the case with k_{AS} = 0.75, k_{AB} = 0.15; Figure 1a), 15.16 nm (in the case with k_{AS} = 0.6, k_{AB} = 0.3; Figure 2a), 10 nm (in the case with k_{AS} = 0.45, k_{AB} = 0.45; Figure 2e). Therefore, the average lateral sizes of clusters of component A formed on the substrate (and calculated in the plane z = 6) decrease from 17.8 nm to 10 nm as the value of the sticking coefficient, k_{AS}, is lowered from 0.75 to 0.45 (keeping the sum $k_{AS} + k_{BS}$ constant). As can be seen in Figures 1b,c and 2b,c,f,g, the changes in the sticking coefficients related to the substrate do not significantly influence the growth dynamics and phase structures obtained in the later growth stages. In the vertical cross sections in Figures 1d and 2d,h, we notice that the branching process of the relatively large clusters of component A (formed on the substrate in the initial growth stages) occurred in all three cases presented. The only difference between those cases is the number of elongated nanoparticles of component A connected to the large basic clusters and extending from those clusters to the surfaces of the grown films. If the lateral dimensions of any basic cluster of component A are smaller, then fewer elongated nanoparticles can grow from that basic large cluster because, as can be seen in Figures 1c and 2c,g, the lateral dimensions of nanoparticles of component A in the plane z = 18 (the layer near the surface of the film) did not change significantly as the value of the sticking coefficient k_{AS} was varied.

We can conclude that the branching mechanism observed in the cases in Figures 1 and 2 consists of two main steps: the first is the formation of a relatively large cluster of a component that makes up the branching phase. The second step is the division process of that large cluster into smaller clusters (with respect to their lateral dimensions) as a film thin grows thicker, as well as the formation of nanocolumns, elongated in the growth direction, extending from the initial large cluster to the surface of the grown film. We can presume that the first step should be achieved by any process or effect of interaction between the phase (branching phase) and the substrate material, which can result in relatively large lateral dimensions of clusters formed on the substrate. However, that effect must disappear in the later growth stages when the substrate is covered with a deposited film, and the growth conditions in the later stages must be favorable to the formation of nanoparticles with a smaller lateral size to achieve the branching process. The important role of the substrate material is also supported by the fact that the formation of such branching structures in yttrium-stabilized zirconia (YSZ) thin films grown by using e-

beam deposition technique [22] was only observed when the film was deposited on a porous Ni-YSZ substrate.

As previously revealed, the formation of relatively large nanoclusters on the substrate during early growth stages is the first necessary condition for the branching process to occur through the mechanism described. Figure 3 shows the plot of average lateral grain size near the substrate versus the value of the diffusion coefficient of component A on the substrate material, D_{AS}. The average grain sizes were assessed at the following values of D_{AS} (in m²/s): 8.8×10^{-17}, $4.4.8 \times 10^{-17}$, 2.2×10^{-17}, 8.8×10^{-18}, and 8.8×10^{-19} (the structures obtained with the values of 8.8×10^{-17}, 2.2×10^{-17}, and 8.8×10^{-19} are given in Figure 1). According to Figure 3, the average lateral grain size near the substrate monotonically increases with the increase in the diffusion coefficient, D_{AS}. The relationship between the average lateral grain size and the diffusion coefficient given in Figure 3 can be approximated by a logarithmic trendline, which, as shown by the value of R^2 in Figure 3, explains 95.6 of the variation of the average lateral grain size related to the changes in the diffusion coefficient, D_{AS}, in the given range. An analysis of the structures obtained with all five diffusion coefficient D_{AS} reveals that, only at the lowest value of D_{AS} (at 8.8×10^{-19} m²/s), no branching process was observed. At the lowest value of D_{AS} used, the formation of clusters with a size of only 5.2 nm, on average, was observed on the substrate material in the early growth stages. The further increase in the diffusion coefficient D_{AS} from 8.8×10^{-18} m²/s to 8.8×10^{-17} m²/s resulted in an increase in the average cluster size (of component A) from 9.5 to 18 nm; the average cluster sizes in that range were favorable for the branching process to occur.

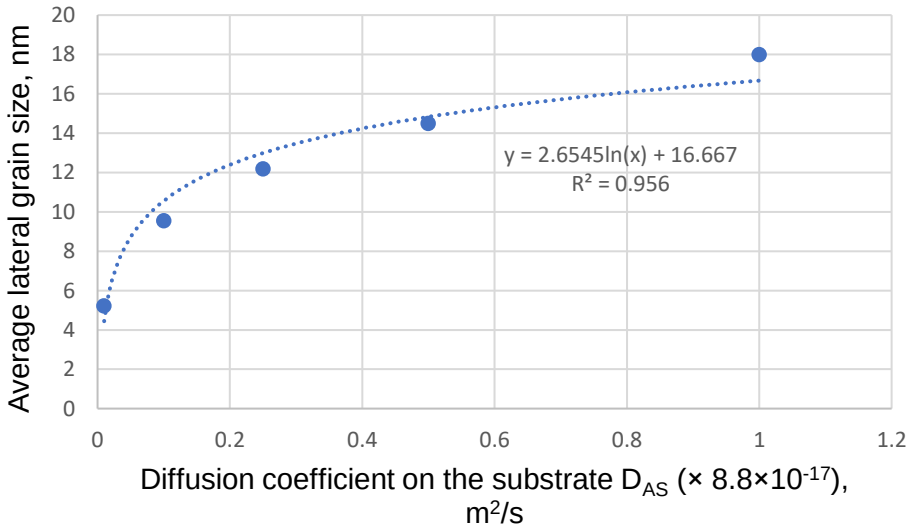

Figure 3. Plot of average lateral grain size near the substrate versus diffusion coefficient of component A on the substrate, D_{AS}.

Figure 4 shows the plot of average lateral cluster size (of component A) near the substrate versus difference $k_{AS} - k_{BS}$. The condition $k_{AS} + k_{BS} = 0.9$ was maintained when the difference between k_{AS} and k_{BS} was varied. The average lateral grain sizes were assessed at the following values of the differences between k_{AS} and k_{BS}: −0.6, −0.3, 0, 0.3, and 0,6. Therefore, the difference $k_{AS} - k_{BS} = -0.6$ corresponds to the pair of $k_{AS} = 0.15$, $k_{BS} = 0.75$, $k_{AS} - k_{BS} = 0$ corresponds to $k_{AS} = 0.45$ and $k_{BS} = 0.45$, $k_{AS} - k_{BS} = 0.6$ corresponds to $k_{AS} = 0.75$ and $k_{BS} = 0.15$, etc. The other model parameters were the same as those used to calculate the structure given in Figure 1a–d. Figure 4 shows a monotonic relationship between the average grain size near the substrate and the difference $k_{AS} - k_{BS}$; such a relationship confirms that the lateral sizes of nanoclusters near the substrate can be influenced by the values of the sticking coefficients. According to Figure 4, the increase in the difference $k_{AS} - k_{BS}$ from

−0.6 to 0 increases the average lateral size of nanoclusters from 8.6 to 10 nm, but the further increase in the difference $k_{AS} - k_{BS}$ from 0 to 0.6 results in a significantly greater increase in the average cluster size from 10 to 18 nm. Such an asymmetric relationship should be highly conditioned by the use of different relative fluxes of depositing species (i_A = 0.2666 s^{-1}, i_B = 0.5333 s^{-1}) and different diffusion coefficients on the substrate material, D_{AS} and D_{BS}. From an analysis of the structures obtained with all five differences $k_{AS} - k_{BS}$ considered, we noticed that the branching process was observed in all the cases, but an increase in the average lateral cluster size near the substrate caused changes in the patterns of the branching structures obtained. A larger lateral cluster size near the substrate usually had more elongated nanocolumns extending from that cluster to the surface of the film.

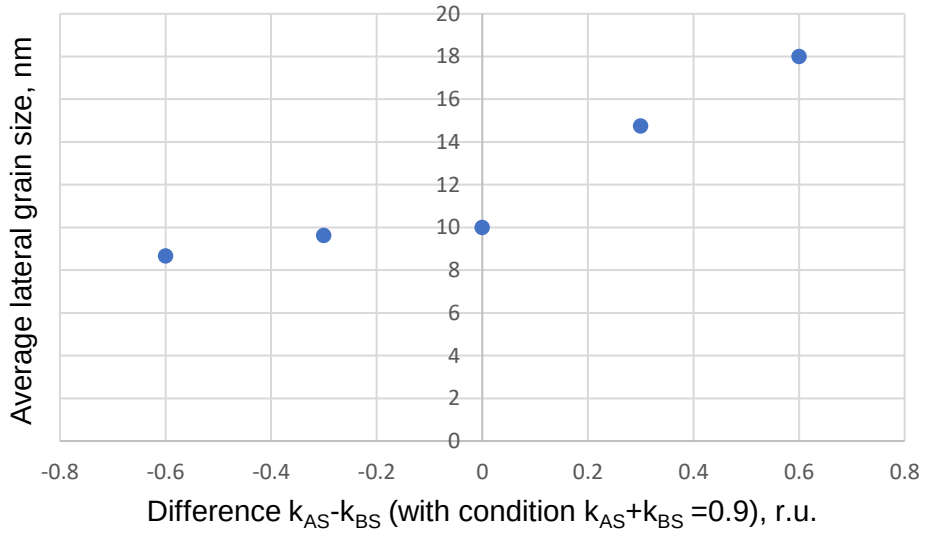

Figure 4. Plot of average lateral grain size near the substrate versus difference $k_{AS} - k_{BS}$ with condition $k_{AS} + k_{BS}$ = 0.9.

Figure 5 presents horizontal and vertical cross sections obtained by using various pairs of values of sticking coefficients k_{AA} and k_{AB} (k_{AA} is the sticking coefficient of component A to pure phase A, and k_{AB} is the sticking coefficient of component A to pure phase B). The horizontal cross sections are given through the same planes as earlier. The vertical cross sections are given through the planes x = 25 in Figure 5d, x = 15 in Figure 5h, and y = 25 in Figure 5l. Both sticking coefficients were varied identically; the values k_{AA} = 0.75 and k_{AB} = 0.75 were used to calculate the images given in Figure 5a–d, the values k_{AA} = 0.5 and k_{AB} = 0.5 were used to obtain the structure provided in Figure 5e–h, and the values k_{AA} = 0.25 and k_{AB} = 0.25 were used to obtain Figure 5i–l. Therefore, from Figure 5a–d,i–l the sticking coefficients, k_{AA} and k_{AB}, were reduced monotonically. In Figure 5a,c,i, where the concentration plots of component A near the substrate are presented, we notice that the changes in the sticking coefficients, k_{AA} and k_{AB}, do not have much of an influence on the structures formed on the substrate material in the initial growth stages. As shown by Figure 5a,e,i, the laterally large clusters of phase A are formed on the substrate in all three cases given, which is not an unexpected result because the sticking coefficients, k_{AA} and k_{AB}, influence the adsorption rates of type-A particles on only pure phase A and pure phase B (and not on the substrate material), respectively, and those coefficients should have a relatively low influence on the structures formed on the substrate. The effect of the sticking coefficients, k_{AA} and k_{AB}, on the phase structures formed is noticeable in the images given in Figure 5b,c,f,g,j,k, where the distributions of component A in the mid-depth and surface layers of the films, , respectively, are provided.

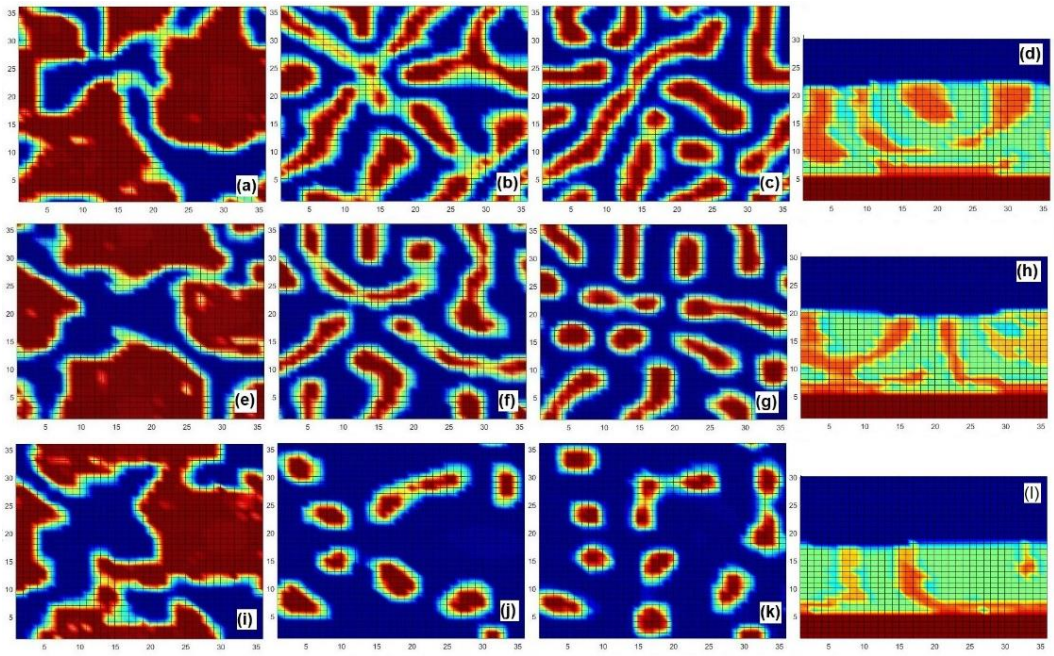

Figure 5. Horizontal cross sections through the planes z = 6 (**a**,**e**,**i**), z =12 (**b**,**f**,**j**), and z = 18 (**c**,**g**,**k**) and vertical cross sections through the planes x = 25 (**d**), x = 15 (**h**), and y = 25 (**l**) obtained with the following sticking coefficients: k_{AA} = 0.75, k_{AB} = 0.75 (**a**–**d**), k_{AA} = 0.5, k_{AB} = 0.5 (**e**–**h**), k_{AA} = 0.25, and k_{AB} = 0.25 (**i**,**j**,**k**,**l**).

As can be seen in those images, the fractions of component A in the given layers visually decrease as the values of the two sticking coefficients are lowered from 0.75 to 0.5 and from 0.5 to 0.25, respectively. As can be seen in Figure 5b,c,f,g,j,k, the lateral dimensions and aspect ratios of nanoparticles made of component A (with respect to the planes considered) are highly influenced by the values of the sticking coefficients, k_{AA} and k_{AB}. In Figure 5j,k, we notice that at the lowest sticking coefficients used, the concentrations of component A in the layers considered are relatively low, and the aspect ratios of nanoparticles made of component A with respect to the planes considered are near the ratio 1:1 for almost all nanoparticles. In Figure 5b,c,f,g we notice that at the higher values of the sticking coefficients used, the dimensions and aspect ratios of nanoparticles of component A with respect to the planes considered are significantly different than in the case with the lowest values of the sticking coefficients. In the case with the highest two values of both sticking coefficients, k_{AA} and k_{AB}, we observe an increase in the lateral dimensions of nanoparticles (with respect to planes considered) of component A, and those increases in the lateral dimensions of nanoparticles are mostly seen in the only one direction, which results in higher deviations of the aspect ratios of nanoparticles made of component A from the ratio 1:1. As can be seen in Figure 5a,e,i, the formation of relatively large (in their lateral dimensions) clusters made of component A on the substrate in the initial growth stages should be favorable to the development of branching structures in all the cases presented; however, as can be seen from Figure 5, the branching structures with elongated nanoparticles made of component A, extending from basic large clusters of component A lying on the substrate to the surface of the grown film, are observed in the cases with lower values of sticking coefficients k_{AA} and k_{AB}. Therefore, a relatively low amount of component A being adsorbed in the later growth stages when the substrate is fully covered with the depositing species is an important condition for the branching process to occur. If the amount of component A adsorbed in the later growth stages is too high, we do not observe any elongated nanoparticles of component A extending from the substrate to the surface of the grown film, which would be an essential feature of the branching structures being considered; however, in those cases, during the later growth stages, we

observe the formation of phase structures containing some higher-dimension nanoparticles of component A. The fraction of particles of component A adsorbed in the later growth stages should not be too low because a lower amount of component A would result in a lower number of branching nanocolumns, which is also an important feature of branching structures.

To provide a better representation of the nanostructures modeled, Figure 6 shows three-dimensional plots of nanoclusters made of component A obtained with different diffusion coefficients of component A on the substrate material, D_{AS}. The values of D_{AS} were as follows: $D_{AS} = 8.8 \times 10^{-17}$ m^2/s (a), $D_{AS} = 2.2 \times 10^{-17}$ m^2/s (b), and $D_{AS} = 8.8 \times 10^{-19}$ m^2/s (c). The cross-sectional views obtained with those diffusion coefficients are presented in Figure 1; the images given in Figures 1 and 6 were drawn from the same modeling data. Component B and the substrate were removed from the given plots to obtain a better visual representation of nanoclusters made of component A, as we are focused mainly on the form of those clusters. As can be seen in the three-dimensional plots given in Figure 6, some areas near the substrates (the top of the substate is always located at z = 5) are obscured by other parts of nanoclusters, so those three-dimensional plots should be examined together with the respective cross-sectional images given in Figure 1. Figure 6 confirms that the growth of branching structures made of component A was observed only at the two highest diffusion coefficient D_{AS} (8.8×10^{-17} m^2/s (a) and 2.2×10^{-17} m^2/s), whereas at the lowest value of D_{AS}, the growth of branching structures was inhibited.

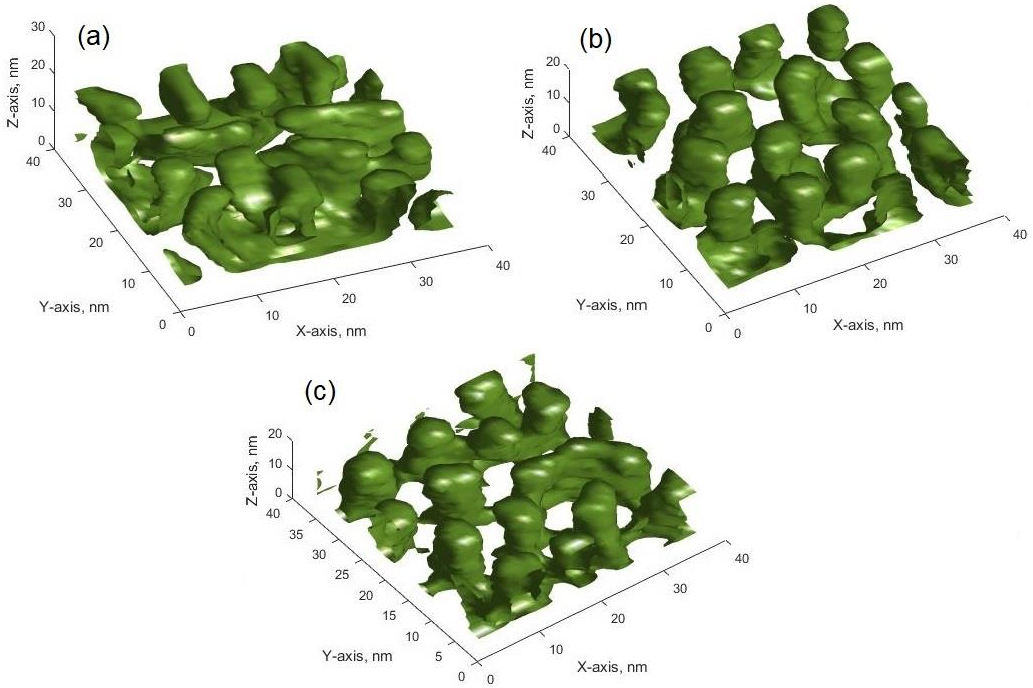

Figure 6. Three-dimensional plots of nanoclusters made of component A obtained with different diffusion coefficient D_{AS}; the values of D_{AS} were as follows: $D_{AS} = 8.8 \times 10^{-17}$ m^2/s (**a**), $D_{AS} = 2.2 \times 10^{-17}$ m^2/s (**b**), and $D_{AS} = 8.8 \times 10^{-19}$ m^2/s (**c**).

To gain a better understanding of the mechanism and growth of branching structures in time, Figure 7 provides three-dimensional plots of nanoclusters made of component A observed at different growth times. The plots are represent the following growth times: 0.1T (a), 0.2T (b), 0.3T (c), and 0.5T (d), where T is the total growth time modeled. The plots given in Figures 1e–h, 6b, and 7 were taken from the same numerical experiment, but they show the structures observed at different growth times. Figure 6b represents the structure observed at the growth time, T. Figure 7a shows a group of nanoislands of component A formed on the substrate material at the growth time 0.1T. The heights of those nanoislands vary from 2 to 2.5 nm. Figure 7a shows only nanoclusters made of component A, but the

analysis of the distributions of both growing phases A and B showed the presence of nanoparticles of component B formed all around the nanoislands of component A at the growth time 0.1T. As shown by Figure 7a, all the upper surfaces of the nanoislands made of component A are convex or flat at the growth time 0.1T. However, as can be noticed from Figure 7b, the certain areas of the upper surfaces of nanoislands of component A became concave until growth time 0.2T (those nanoislands are indicated by arrows in Figure 7b). From Figure 7b, it can be seen that the nanoclusters of component A with relatively large lateral dimensions remained convex in the outer areas of their surfaces, whereas the inner areas of their surfaces tended to become concave. The analysis of the distributions of both growing phases A and B revealed the nucleation of nanoclusters made of component B on those inner areas of the nanoislands of component A. Therefore, such a change in the form of nanoclusters of component A from convex to concave (in the inner areas of the nanoclusters) is conditioned by the nucleation of phase B on the respective nanoislands of component A. That nucleation of phase B on nanoislands of component A is more likely on inner areas of nanoislands (of component A) because if we consider a pure nanoisland of component A with nanoparticles of component B formed all around that nanoisland, those inner areas are relatively far from any cluster made of component B, so when the lateral dimensions of that nanoisland of component A are large enough, particles of type B adsorbed on inner parts of that nanoisland of component A may be unable to diffuse long enough to reach any nanocluster of component B situated around that nanoisland of component A. In this way, the nucleation of phase B on nanoislands of component A is promoted. Such a process of nucleation can only occur when the formation of relatively large clusters is favorable in the initial growth stages when nanoislands grow on the substrate, whereas the formation of nanoparticles with smaller lateral dimensions is favorable in the later growth stages. Such a change in the lateral dimensions of nanoclusters is influenced by the differences between the diffusivities (and sticking coefficients) of depositing species on the substrate material and pure their phases. As shown in Figure 7c, considering the relatively wide nanoislands of component A formed on the substrate, phase A continues growing primarily on outer parts of those nanoislands (although, as shown by Figure 6a, phase A may continue growing not only on outer parts of nanoislands but also on inner parts if the lateral dimensions of a nanoisland are large enough). In those areas, the growth of phase A can be still favorable because any particle of type B adsorbed to outer areas of a nanoisland of component A can easily diffuse to reach clusters made of component B, which are formed all around any nanoisland of component A or are nucleated on the inner areas of any sufficiently large nanoisland of component A. In Figure 7c, we notice that on some outer parts of the nanoislands of component A (where the growth of phase A was favorable), phase A grows slower than on the others, which, as shown by Figure 7d, leads to the division of the nanoclusters made of phase A into smaller cluster. Those smaller cluster continue growing as nanocolumns extending from the large initial clusters to the surface of the grown film. Such a branching process is promoted (in the later growth stages) by decreasing the amount of component A adsorbed in the later growth stages. In our model, the amount of component A adsorbed in the later growth stages is simply determined by the sticking coefficients k_{AA} and k_{AB} (the sticking coefficients of component A to pure phase A and B, respectively).

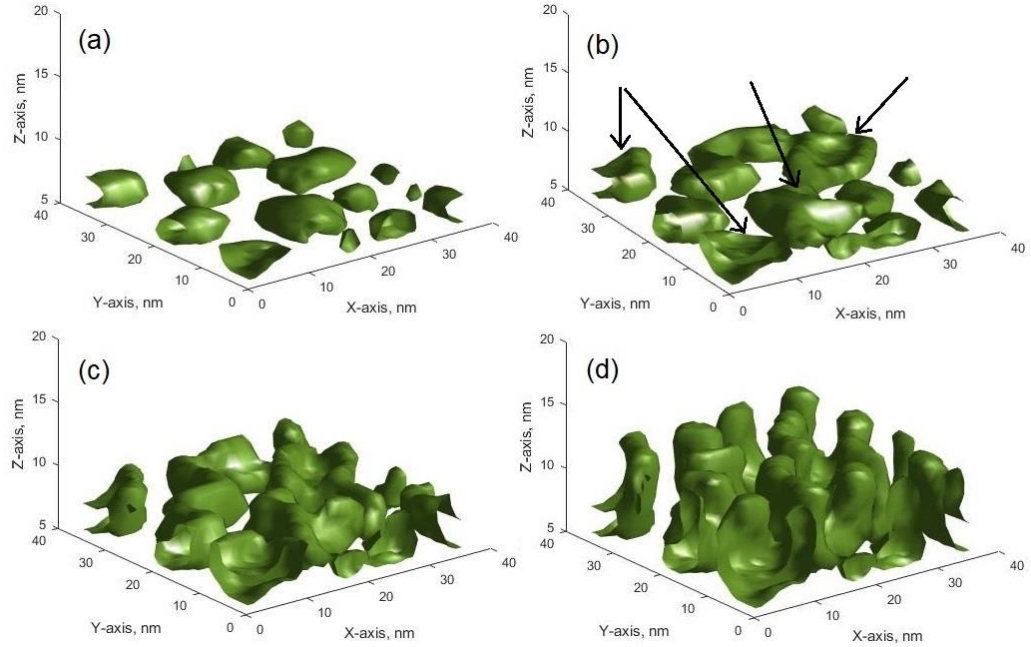

Figure 7. Three-dimensional plots of nanoclusters made of component A observed at different growth times. The growth times were as follows: 0.1T (**a**), 0.2T (**b**), 0.3T (**c**), and 0.5T (**d**).

The influence of substrate temperature on the branching process can be discussed on the basis of this study, as well as our previous works [13,20]. If we consider the temperature range $0.2T_m < T$ (T_m is melting temperature), diffusion coefficients increase exponentially with the substrate temperature, T_S, in that range. According to the Langmurian temperature dependence of adsorption processes, the growth rate is proportional to $1/\sqrt{T_s}$. Therefore, diffusion coefficients increase with an increase in the substrate temperature, and the growth rate decreases with an increase in the substrate temperature. In [13], it is shown that the average lateral size of nanoclusters increases with an increase in the substrate temperature. In [13], it is also shown that the average lateral size of nanoclusters increases with a decrease in the growth rate. Therefore, based on the findings of this and other works [13,20], a relatively high substrate temperature (assuming both dependencies of diffusivities and the growth rate on substrate temperature specified) should be favorable for the formation of laterally large clusters in initial growth stages, but high substrate temperatures are not favorable for the formation of nanocolumns with relatively small lateral dimensions. This leads to the conclusion that relatively high substrate temperatures in initial growth stages and lower substrate temperatures in later growth stages should be favorable for the formation of branching structures.

4. Conclusions

(1). The modeling results revealed the possible mechanism through which the formation of branching structures with nanocolumns elongated in the growth direction and extending from a relatively large cluster formed on the substrate to the surface of a grown film could be achieved.

(2). The growth mechanism of branching structures can be divided into the two main steps. The first step is the growth of a relatively large cluster (of a component that makes up the branching phase) on the substrate. The second step is the division process of that large cluster into smaller clusters as a film thin grows thicker, as well as the formation of nanocolumns elongated in the growth direction and extending from the initial large cluster to the surface of the grown film.

(3). The modeling results showed that relatively high values of diffusivities and sticking coefficients of respective components on the substrate material were favorable factors

for the formation of large clusters on the substrate. The lower values of diffusivities and sticking coefficients of respective components on the phases made of depositing species (in comparison to those on the substrate material) are the factors that could resulting in conditions favorable to the formation of clusters with smaller lateral dimensions in the later growth stages, which promoted the branching process of large clusters formed in the early growth stages.

Author Contributions: Conceptualization, A.G. (Arvaidas Galdikas), M.G., A.G. (Artūras Grigaliūnas), and G.K.; methodology, G.K. and A.G. (Arvaidas Galdikas); software, G.K.; validation, G.K. and A.G. (Arvaidas Galdikas); investigation, G.K., M.G., A.G. (Arvaidas Galdikas), and A.G. (Artūras Grigaliūnas); writing—original draft preparation, G.K. and A.G. (Arvaidas Galdikas); writing—review and editing, G.K., M.G., A.G. (Arvaidas Galdikas), and A.G. (Artūras Grigaliūnas); visualization, G.K. and A.G. (Arvaidas Galdikas); supervision, A.G. (Arvaidas Galdikas); funding acquisition, A.G. (Arvaidas Galdikas), M.G. and G.K. All authors have read and agreed to the published version of the manuscript.

Funding: This project received funding from the European Regional Development Fund (Grant No. 01.2.2-LMT-K-718-01-0071) under grant agreement with the Research Council of Lithuania (LMTLT).

Institutional Review Board Statement: Not applicable.

Informed Consent Statement: Not applicable.

Data Availability Statement: Not applicable.

Acknowledgments: The authors would like to express their gratitude to the following individuals for their expertise and contribution to the manuscript: G. Laukaitis, T. Moskaliovienė, K. Bočkutė, D. Virbukas, M. Sriubas, and V. Kavaliūnas.

Conflicts of Interest: The authors declare no conflict of interest.

References

1. Tamulevičius, S.; Meškinis, Š.; Tamulevičius, T.; Rubahn, H.G. Diamond like carbon nanocomposites with embedded metallic nanoparticles. *Rep. Prog. Phys.* **2018**, *81*, 024501. https://doi.org/10.1088/1361-6633/aa966f.
2. Nan, C.-W.; Jia, Q. Obtaining ultimate functionalities in nanocomposites: Design, control, and fabrication. *MRS Bull.* **2015**, *40*, 719–724. https://doi.org/10.1557/mrs.2015.196.
3. Kovács, G.J.; Sáfrán, G.; Geszti, O.; Ujvári, T.; Bertóti, I.; Radnóczi, G. Structure and mechanical properties of carbon-nickel and CNx-nickel nanocomposite films. *Surf. Coat. Technol.* **2004**, *180–181*, 331–334. https://doi.org/10.1016/j.surfcoat.2003.10.081.
4. Abrasonis, G.; Kovács, G.J.; Ryves, L.; Krause, M.; Mücklich, A.; Munnik, F.; Oates, T.W.H.; Bilek, M.M.M.; Möller, W. Phase separation in carbon-nickel films during hyperthermal ion deposition. *J. Appl. Phys.* **2009**, *105*, 083518. https://doi.org/10.1063/1.3110187.
5. Schultes, G.; Schmid-Engel, H.; Schwebke, S.; Werner, U. Granular metal-carbon nanocomposites as piezoresistive sensor films—Part 1: Experimental results and morphology. *J. Sens. Sens. Syst.* **2018**, *7*, 1–11. https://doi.org/10.5194/jsss-7-1-2018.
6. Park, J.H.; Ahn, J.; Yoon, K.J.; Kim, H.; Ji, H.-I.; Lee, J.-H.; Han, S.M.; Son, J.-W. Columnar Grain Size Effect on Cross-Plane Conductivity of Yttria-Stabilized Zirconia Thin Films. *J. Electrochem. Soc.* **2018**, *165*, F671–F676. https://doi.org/10.1149/2.0961809JES.
7. Wang, W.; Ji, L.; Li, H.; Zhou, H.; Chen, J. Self-organized formation of nano-multilayer structure in the carbon-copper thin film during reactive magnetron sputtering deposition process. *J. Alloys Compd.* **2017**, *722*, 242–249. https://doi.org/10.1016/j.jallcom.2017.06.006.
8. Armelao, L.; Barreca, D.; Bottaro, G.; Gasparotto, A.; Gross, S.; Maragno, C.; Tondello, E. Recent trends on nanocomposites based on Cu, Ag and Au clusters: A closer look. *Coord. Chem. Rev.* **2006**, *250*, 1294–1314.
9. Gao, C.; Lyu, F.; Yin, Y. Encapsulated Metal Nanoparticles for Catalysis. *Chem. Rev.* **2021**, *121*, 834–881. https://doi.org/10.1021/acs.chemrev.0c00237.
10. Derby, B.; Cui, Y.; Baldwin, J.K.; Misra, A. Effects of substrate temperature and deposition rate on the phase separated morphology of co-sputtered, Cu-Mo thin films. *Thin Solid Films* **2018**, *647*, 50–56. https://doi.org/10.1016/j.tsf.2017.12.013.
11. Ankit, K.; Derby, B.; Raghavan, R.; Misra, A.; Demkowicz, M.J. 3-D phase-field simulations of self-organized composite morphologies in physical vapor deposited phase-separating binary alloys. *J. Appl. Phys.* **2019**, *126*, 075306. https://doi.org/10.1063/1.5110410.
12. Perzynski, K.; Cios, G.; Szwachta, G.; Bała, P.; Madej, L. Numerical study on the dependency of microstructure morphologies of pulsed laser deposited tin thin films and the strain heterogeneities during mechanical testing. *Materials* **2021**, *14*, 1705. https://doi.org/10.3390/ma14071705.

13. Galdikas, A.; Sriubas, M.; Kairaitis, G.; Virbukas, D.; Bockute, K.; Galdikas, M.; Moskalioviene, T.; Laukaitis, G. Investigation of morphology of aluminum co-doped scandium stabilized zirconia (ScALSZ) thin films. *Coatings* **2022**, *12*, 31. https://doi.org/10.3390/coatings12010031.
14. Powers, M.; Stewart, J.A.; Dingreville, R.; Derby, B.K.; Misra, A. Compositionally-driven formation mechanism of hierarchical morphologies in co-deposited immiscible alloy thin films. *Nanomaterials* **2021**, *11*, 2635. https://doi.org/10.3390/nano11102635.
15. Bouaouina, B.; Mastail, C.; Besnard, A.; Mareus, R.; Nita, F.; Michel, A.; Abadias, G. Nanocolumnar TiN thin film growth by oblique angle sputter-deposition: Experiments vs. simulations. *Mater. Des.* **2018**, *160*, 338–349. https://doi.org/10.1016/j.matdes.2018.09.023.
16. To, T.B.T.; Aarão Reis, F.D.A. Domain formation in the deposition of thin films of two-component mixtures. *J. Alloys Compd.* **2020**, *835*, 155093. https://doi.org/10.1016/j.jallcom.2020.155093.
17. Mińkowski, M.; Załuska-Kotur, M.A.; Kret, S.; Chusnutdinow, S.; Schreyeck, S.; Brunner, K.; Molenkamp, L.W.; Karczewski, G. Self-organization process in crystalline PbTe/CdTe multilayer structures: Experiment and Monte Carlo simulations. *J. Alloys Compd.* **2018**, *747*, 809–814. https://doi.org/10.1016/j.jallcom.2018.03.079.
18. Zhou, X.; Yu, X.; Jacobson, D.; Thompson, G.B. A molecular dynamics study on stress generation during thin film growth. *Appl. Surf. Sci.* **2019**, *469*, 537–552. https://doi.org/10.1016/j.apsusc.2018.09.253.
19. Stewart, J.A.; Dingreville, R. Microstructure morphology and concentration modulation of nanocomposite thin-films during simulated physical vapor deposition. *Acta Mater.* **2020**, *188*, 181–191. https://doi.org/10.1016/j.actamat.2020.02.011.
20. Kairaitis, G.; Galdikas, A. Modelling of phase structure and surface morphology evolution during compound thin film deposition. *Coatings* **2020**, *10*, 1077. https://doi.org/10.3390/coatings10111077.
21. Lu, Y.; Derby, B.; Sriram, H.; Kadirvel, K.; Wang, C.; Liu, X.; Misra, A.; Wang, Y. Microstructure development and morphological transition during deposition of immiscible alloy films. *Acta Mater.* **2021**, *220*, 117313. https://doi.org/10.1016/j.actamat.2021.117313.
22. Laukaitis, G.; Dudonis, J.; Milčius, D. Microstructure and surface morphology of YSZ thin films deposited by e-beam technique. *Appl. Surf. Sci.* **2008**, *254*, 2980–2987. https://doi.org/10.1016/j.apsusc.2007.10.041.
23. Laukaitis, G.; Dudonis, J.; Milcius, D. Morphology and growth of e-beam deposited YSZ thin films. *Vacuum* **2007**, *81*, 1288–1291. https://doi.org/10.1016/j.vacuum.2007.01.030.
24. Cahn, J.W.; Hilliard, J.E. Free energy of a nonuniform system. I. Interfacial free energy. *J. Chem. Phys.* **1958**, *28*, 258–267. https://doi.org/10.1063/1.1744102.
25. Kairaitis, G.; Grigaliūnas, A.; Baginskas, A.; Galdikas, A. Kinetic modeling of phase separation and surface segregation in growing a-C:Ni thin films. *Surf. Coat. Technol.* **2018**, *352*, 120–127. https://doi.org/10.1016/j.surfcoat.2018.08.012.
26. Galdikas, A.; Pranevičius, L. Surface composition changes of ternary alloys in the non-steady state regime of preferential sputtering. *Nucl. Instrum. Methods Phys. Res. Sect. B Beam Interact. Mater. Atoms* **2000**, *164*, 868–872. https://doi.org/10.1016/S0168-583X(99)01115-5.
27. Kairaitis, G.; Galdikas, A. Phase separation during thin film deposition. *Comput. Mater. Sci.* **2014**, *91*, 68–74. https://doi.org/10.1016/j.commatsci.2014.04.034.
28. Atzmon, M.; Kessler, D.A.; Srolovitz, D.J. Phase separation during film growth. *J. Appl. Phys.* **1992**, *72*, 442–446. https://doi.org/10.1063/1.351872.
29. Adams, C.D.; Srolovitz, D.J.; Atzmon, M. Monte Carlo simulation of phase separation during thin-film codeposition. *J. Appl. Phys.* **1993**, *74*, 1707–1715. https://doi.org/10.1063/1.354825.